



Dynamic model on thermally induced characteristics of ball screw systems

Tie-jun Li¹ · Kuo Liu²

Received: 27 October 2018 / Accepted: 15 April 2019 / Published online: 8 May 2019
© Springer-Verlag London Ltd., part of Springer Nature 2019

Abstract

Ball screws used for high-speed feed systems generate friction heat, which affects the preload and supporting system stiffness, and further, the dynamic characteristics of the screw system are modified and negative effects on the positioning accuracy are produced. Therefore, a thermal dynamic model for investigating dynamic performance variation with temperature is needed. First, a new dynamic temperature model of a hollow cylinder with varied heat flow was proposed based on the heat transfer theory. By using the thermocouples to read the real-time surface temperatures of heat sources, this model can be used to obtain the real-time temperature field of the supporting bearings and nut, and by using the FOCAS function to read the real-time position of nut, a finite difference heat transfer model with real-time moving heat sources was established. Based on this model, the dynamic thermally induced preload and stiffness models of the system were obtained. Second, a real-time thermal dynamic model of the ball screw system was achieved. Finally, an inverse identification method of the heat excitation was proposed. Through measuring dynamic characteristics of the feed system in machine tools, the real-time thermal dynamic models of the screw system were validated. It provided the theoretical and practical foundation for real-time monitoring and controlling of dynamic characteristics of preloaded ball screw systems.

Keywords Ball screw system · Thermally induced dynamic characteristics · Supporting system stiffness · Preload · Heat transfer

Nomenclature

k_b	Axial stiffness of the support bearing
F_0	Initial tensile preload of the screw
ΔF_0	Lessened tensile preload of the temperature increasing
$\Delta T(x, t)$	Temperature increment
S_S	Section area of the screw
E	Modulus of elasticity
α_S	Expansion coefficient of the screw shaft
L	Length of the screw
x	Position of the table in the screw

k_e	Axial equivalent stiffness for the supporting bearings and the screw
d_s	Diameter of the screw
F_{n0}	Initial compressive preload between the screw and the nut
k_n	Screw-nut stiffness
F_{a0}	Compressive preload of the moving nut
k_s	Axial stiffness for the screw
K	Rate stiffness of the screw-nut
ε	Constant of the load
C_a	Rate equivalent dynamic load of the screw
F_{ap}	Axial load applied on the working table
δ_{b0}	Elastic axial deformation of the fastened supporting bearing
F_{b0}	Compressive preload of the fastened supporting bearing
d_b	Diameter of balls of the supporting bearing
β_b	Contact angle of the supporting bearing
Q	Axial load of each ball of the supporting bearing
$[M]$	System mass matrices
$[C]$	System damping matrices
$[K]$	System stiffness matrices

✉ Tie-jun Li
litiejun@syuct.edu.cn

¹ Department of Mechanical Engineering, Shenyang University of Chemical Technology, Shenyang 110142, China

² Key Laboratory for Precision and Non-traditional Machining Technology of Ministry of Education, Dalian University of Technology, Dalian 116024, China

$[F]$	Excitation force vector
$[X]$	Displacement vector
$T(x, t)$	Temperature distribution of the screw, dependent on time and distance
k	Thermal conductivity of the screw
ρ	Screw density
c	Heat capacity
h	Convective coefficient
$T_{\text{air}}(t)$	Temperature of the ambient air
$T_{cb1}(t)$	Key point temperature of the screw connecting with the bearing 1
$T_{cb2}(t)$	Key point temperature of the screw connecting with the bearing 2
$T_{cn}(t)$	Key point temperature of the screw connecting with the moving-nut
P	Perimeter of the screw
A_c	Cross-sectional area of the screw
S	Feed stroke

1 Introduction

With the development of high-speed and high-precision machine tools, preloaded ball screw feed drive systems are widely used [1, 2], which can increase the axial rigidity, modify the nature frequency in order to avoid the vibration, and improve the manufacturing quality [3, 4]. Hence, the dynamic characteristics of high-speed ball screw systems have attracted the attention of many researchers [5–18]. Erkorkmaz et al. [8] proposed a new method of identifying the dynamic parameters and the friction characteristics of feed drive systems used in machine tools. Jerzy et al. [9] investigated a resonance frequency of ball screw feed drive systems of CNC machine tools. Li et al. [10] presented a modal identification method to investigate the dynamics of machine tool feed drive systems under different feed rates. Feng et al. [11] proposed a lumped dynamic model of the screw system to study preload influences on the dynamic response. Zhou et al. [12] found an accurate relationship between the preload and no-load drag torque. Frey et al. [13] studied the behavior of ball screw feed drives and its dominant influence. Frey et al. [14] found that the preload is one of main parameters of the working performance of ball screws. Vicente et al. [15] proposed a new high-frequency dynamic model of ball screw systems, using this model, the frequency variation of each mode of the systems was investigated under different carriage positions and masses. Wei et al. [16] proposed the kinematics model of the preloaded single-nut high-speed screw. Varanasi et al. [17] proposed a new dynamics model of screw systems that accounts for the screw inertia, compliance, and damping of the main elements. Kamalzadeh et al. [18] proposed a precision control method for ball screw systems and axial vibrations were compensated using the method.

However, preloaded high-speed screw systems generate excessive friction heat; the thermal effects were widely investigated by previous literatures [19–38]. On one hand, with the increase of feed rates, the positioning precision is affected by the thermally induced characteristics [19–22]. In the previous researches, the thermal error accounts for about 40–70% of the whole error of machine tools [23–27]. The methods of reducing thermal error in machine tools are usually the error control and error compensation [22–35]. On the other hand, due to the thermally induced deformation of the screw, the initial preload of the system is changed, which modify the dynamic characteristics, such as the axial rigidity and natural frequency. The preload variation with temperature rise of the double nut preloaded ball screw was analyzed by experiments [36]. A finite element model was proposed to determine the remarkable influence of the preload of a bearing on thermal stabilization of ball screw systems [37]. In literature 38, the remarkable decrease of the preload in preloaded ball screw systems was found by experiments. When the temperature rises by 12–16 K, the preload decreases by 32%.

In summary, many researches focused on the modeling of the thermo-mechanical behavior of ball screw systems. However, most of these researches were carried out to predict and compensate thermal errors [22–35]. Though some of these researchers studied the thermal-preload-mechanical dynamic characteristics by experiments and FEM [33, 36–38], the studies did not consider real-time characteristics of preload ball screw systems with temperature rise.

To better investigate the thermally induced dynamic behavior of the preload ball screw systems and further control the thermal-dynamic behavior, a real-time dynamic model of the preload ball screw systems is necessary, which, however, has been rarely studied by now.

In this paper, the real-time thermal-dynamic model to predict the variation of the preload, stiffness, and natural frequency of preloaded ball screw systems due to temperature increase was proposed by using a heat transfer method. The solution of this model was validated by experiments. It provided the theoretical and practical foundation for real-time monitoring and controlling of dynamic characteristics of preloaded ball screw systems.

2 Thermal dynamic model

The main heat sources in ball screw feed drive systems used for CNC machine tools include the two supporting bearings and moving nut, and the heat rates result from the friction among the components, which are dependent on the feed rate, assembly conditions, and lubricant conditions. Although the system working under the same feed rate, assembly conditions, and lubricant conditions, the thermal deformation also

changes the coherence among the moving nut, the screw, and the supporting bearings.

The thermally induced axial deformation of the screw affects the supporting system stiffness and the friction torque, which changes the dynamic performance of the ball screw system [20].

2.1 Stiffness model of the supporting system

The stiffness of the supporting system of the ball screw feed drive system is composed of the stiffness of the supporting bearings and the stiffness of the screw.

2.1.1 Stiffness of the support bearing

When the ball screw feed drive system is fixed by one end, the stiffness of the support bearing is given by [21]

$$K_b = \frac{3F_{b0}}{\delta_{b0}} \tag{1}$$

The axial deformation of the supporting bearing δ_{b0} in Eq. 1 can be expressed as

$$\delta_{b0} = \frac{0.45}{\sin\beta_b} \left(\frac{Q^2}{d_b} \right)^{1/3} \tag{2}$$

where Q is expressed as

$$Q = \frac{F_{b0}}{n\sin\beta_b} \tag{3}$$

2.1.2 Stiffness of the screw shaft

One end of the ball screw system is fixed, and the other end is free. According to material mechanics, the elongation of the screw caused by the temperature arising makes the tensile preload of the supporting bearing weak. The thermal deformation of the screw changes the coherence of bearings [20], and the tensile preload variation influences the screw stiffness.

According to material mechanics, the lessened tensile preload ΔF_0 due to the temperature increasing is defined as

$$\Delta F_0 = S_s E \Delta L \tag{4}$$

where ΔL denotes the thermal elongation value of the screw shaft.

In order to obtain the thermal elongation value ΔL of the screw shaft, the determination of temperature arising of the screw shaft is necessary.

Real-time modeling of the temperature arising of the screw shaft

In this paper, a new real-time thermal model of multiple

varying and moving heat sources was proposed and used for the screw shaft.

Figure 1 shows the ball screw feed drive system is fastened at the left end, and it is stretched at the other end.

The expression used for calculating heat transfer of the screw can be described as

$$\begin{cases} \frac{\partial^2 T(x, t)}{\partial x^2} - \frac{\rho c}{k} \frac{\partial T(x, t)}{\partial t} + \frac{Ph}{kA_c} (T(x, t) - T_{air}(t)) = 0, x \in [0, L] \\ T(x, 0) = T_{air}(0), x \in [0, L] \\ T(0, t) = T_{cb1}(t_j) \\ T(L, t) = T_{cb2}(t_j) \\ T(x, t) = T_{cn}(x_i, t_j), x \in [0, S] \end{cases} \tag{5}$$

The three key point temperatures $T_{cb1}(t_j)$, $T_{cb2}(t_j)$, and $T_{cn}(t_j)$ of the ball screw connecting with the bearing 1, bearing 2, and nut are important for investigating thermal deformation, preloads, and thermal characteristics. However, these key point temperatures of the system are difficult to be measured, for the temperature sensors could not be put into the prescribed position.

In order to obtain the key point temperatures $T_{cb1}(t_j)$, $T_{cb2}(t_j)$, and $T_{cn}(t_j)$ of the ball screw connecting with the bearing 1, bearing 2, and nut, the model of the temperature arising of the bearing and nut is required.

In this paper, the bearing and nut are simplified as hollow cylinders, and a new real-time temperature model of hollow cylinders is proposed. This model was used for obtaining the key point temperatures $T_{cb1}(t_j)$, $T_{cb2}(t_j)$, and $T_{cn}(t_j)$ of the ball screw contacting with the bearings and moving-nut.

Modeling of real-time temperature field for a hollow cylinder

In order to establish a real-time temperature model of the supporting bearings and moving-nut, the assumptions were as follows [5, 7]:

1. The bearings and screw-nut are treated as hollow cylinders.
2. The friction heat generated by the bearings and screw-nut is uniform.

In this work, a real-time temperature distribution model of a hollow cylinder is proposed according to the heat transfer theory.

Figure 2 shows that the bearings and moving-nut are simplified to be the hollow cylinders with a uniform heat generation rate.

With regard to the convection heat dissipation of the cylinder surfaces, the convection heat loss is treated as a virtual negative heat source.

The transient heat transfer equation for the hollow cylinder with a negative heat source can be expressed as

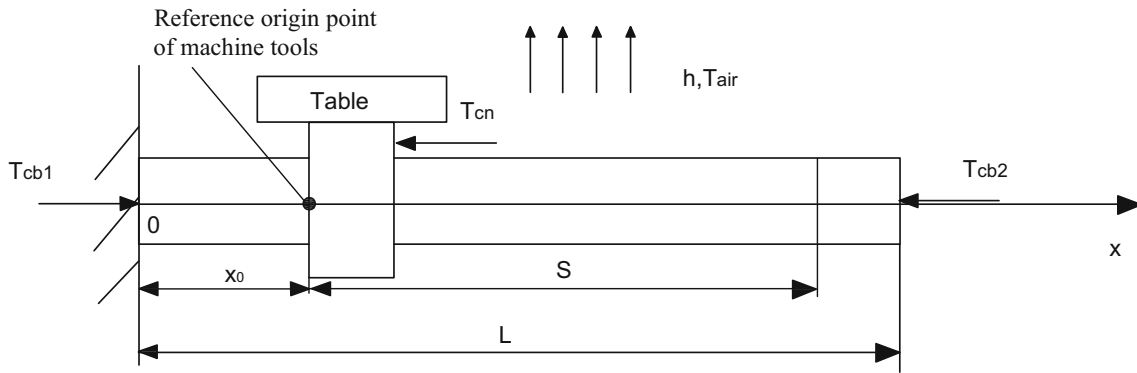


Fig. 1 Heat transfer of the screw

$$\frac{1}{r} \frac{\partial}{\partial r} \left(kr \frac{\partial T(r, t)}{\partial r} \right) = \rho c \frac{\partial T(r, t)}{\partial t} + \dot{\phi} \tag{6}$$

where $\dot{\phi}$ denotes the heat flow of the negative heat source of the cylinder surface convection.

The total heat for the surface convection ϕ_s can be written as

$$\phi_s = P_c dr h_s (T - T_f) \tag{7}$$

where P_c is the circumference of the heat transfer section.

Considering the convection heat transfer of the up, down, and top surfaces, the circumference of the heat transfer section is written as

$$P_c = 2 \left(2\pi r + \frac{W}{2} \right) \tag{8}$$

The negative heat source $\dot{\phi}$ can be rewritten as

$$\dot{\phi} = -\frac{\phi_s}{A_c dr} = -\frac{h_s P_c (T - T_f)}{A_c} \tag{9}$$

where A_c is the area of the heat transfer section.

The area of the heat transfer section A_c is expressed as

$$A_c = 2\pi r W \tag{10}$$

where W denotes the width of the hollow cylinder.

Substituting Eq. 9 into Eq. 6, the temperature model of the hollow cylinder can be rewritten as

$$\frac{1}{r} \frac{\partial}{\partial r} \left(kr \frac{\partial T(r, t)}{\partial r} \right) = \rho c \frac{\partial T(r, t)}{\partial t} - \frac{P_c h_s}{A_c} (T - T_f(t)) \tag{11}$$

where $T(r, t)$ is the temperature distribution of the hollow cylinder, which is the function of time t and the radius r , and h_s is the surface convection coefficient of the hollow cylinder.

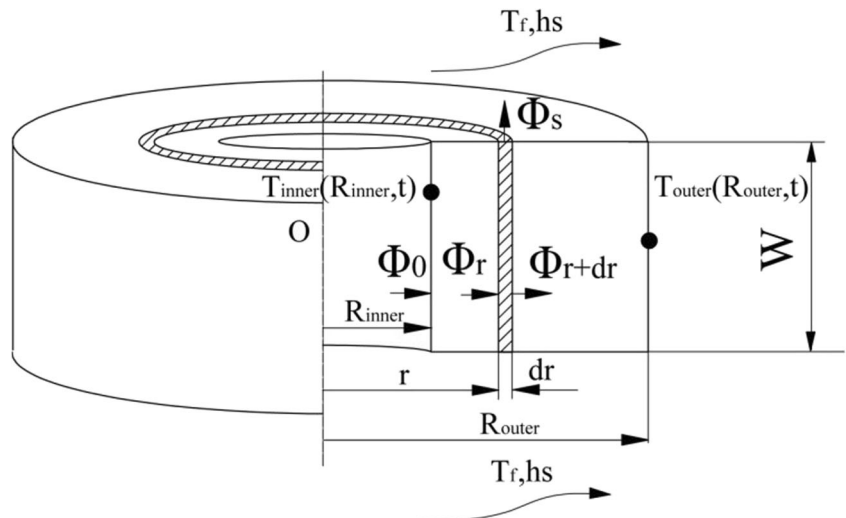
According to the variable separation theory, the temperature distribution of the hollow cylinder $T(r, t)$ is written as

$$T(r, t) = T_r(r) \cdot T_t(t) \tag{12}$$

Temperature of a hollow cylinder always shows a **logarithm** decrease with the radius [39]. In this paper, the function $T_r(r)$ of the position can be written as

$$T_r(r) = \frac{1}{r \ln(R_{out}/R_{in})} \tag{13}$$

Fig. 2 Heat transfer of the hollow cylinder



The temperature of the cylinder always shows an exponential increase with time [39, 40]. In this work, the function $T_t(t)$ of the time is expressed as

$$T_t(t) = A \left(1 - e^{-\frac{t}{B}}\right) \tag{14}$$

where A and B are constants.

Therefore, the transient temperature distribution of the hollow cylinder $T(r, t)$ can be rewritten as

$$T(r, t) = A \frac{1}{r \ln(R_{out}/R_{in})} \left(1 - e^{-\frac{t}{B}}\right) \tag{15}$$

The $\frac{\partial T}{\partial t}$ expression can be derived as

$$\frac{\partial T}{\partial t} = \frac{Ae^{-\frac{t}{B}}}{B} \frac{1}{r \ln(R_{out}/R_{in})} \tag{16}$$

The $\frac{1}{r} \frac{\partial}{\partial r} \left(kr \frac{\partial T(r,t)}{\partial r}\right)$ expression can be derived as

$$\frac{1}{r} \frac{\partial}{\partial r} \left(kr \frac{\partial T(r,t)}{\partial r}\right) = \frac{kA(1 - e^{-\frac{t}{B}})}{r^3 \ln(R_{out}/R_{in})} \tag{17}$$

Substituting Eqs. 16 and 17 into Eq. 11, Eq. 11 can be rewritten as

$$\frac{kA(1 - e^{-\frac{t}{B}})}{r^3 \ln(R_{out}/R_{in})} - \rho c \frac{Ae^{-\frac{t}{B}}}{B} \frac{1}{r \ln(R_{out}/R_{in})} + \frac{P_c h_s (T - T_f)}{A_c} = 0 \tag{18}$$

The analytical solution of Eq. 18 is

$$T = \frac{\rho c A A_c r^2 e^{-\frac{t}{B}} + A B A_c k e^{-\frac{t}{B}} - A B A_c k}{B h_s P_c r^3 \ln(R_{out}/R_{in})} + T_f \tag{19}$$

Equation 19 is adaptive to not only the bearing temperature field but also a nut temperature field.

The real-time surface temperature $T(R_{out}, t_i)$ used for the boundary can be obtained by the thermocouple. The thermocouples on the bearing seat surface and the moving-nut flank surface can be used to collect the real-time temperature and time information. Two sets of data from the measured point of the heat source surface are enough to solve Eq. 19, and then A and B are obtained.

Using the thermocouples to read the surface temperature $T(R_{out}, t_i)$ of the heat source, this real-time model can be used to obtain the real-time temperature $T_{cb1}(t_j)$, $T_{cb2}(t_j)$, and $T_{cn}(t_j)$ of the screw contact surface at the position with the radius R_{in} of the bearings and nut.

The $T(R_{out}, t_i)$ is the real-time temperature for the point measured from the surface of the kinematics pair collected by thermocouples. The $T_{cb1}(t_j)$, $T_{cb2}(t_j)$, and $T_{cn}(t_j)$ are the contacting surface temperatures between the screw shaft and the kinematics pairs.

Hence, this modeling of real-time temperature field for a hollow cylinder can be used to obtain the $T_{cb1}(t_j)$, $T_{cb2}(t_j)$, and $T_{cn}(t_j)$ of the contacting surface temperature between the screw shaft and the bearings and nut.

Numerical solution method of the real-time modeling of the temperature arising of the screw shaft When the contact surface temperatures are obtained, Eq. 5 can be used to calculate the temperature distribution of the screw shaft.

Equation 5 can be solved by the finite difference method. Partition the setting region into mesh by step size of space s and step size of time t . $x_i = i \cdot s$, $t_j = j \cdot \tau$. Node (x_i, t_j) is simplified to (i, j) . $i[1, M - 1]$, $j[1, N - 1]$, M, and N are positive integers, and $T_j^i = T(i, j)$.

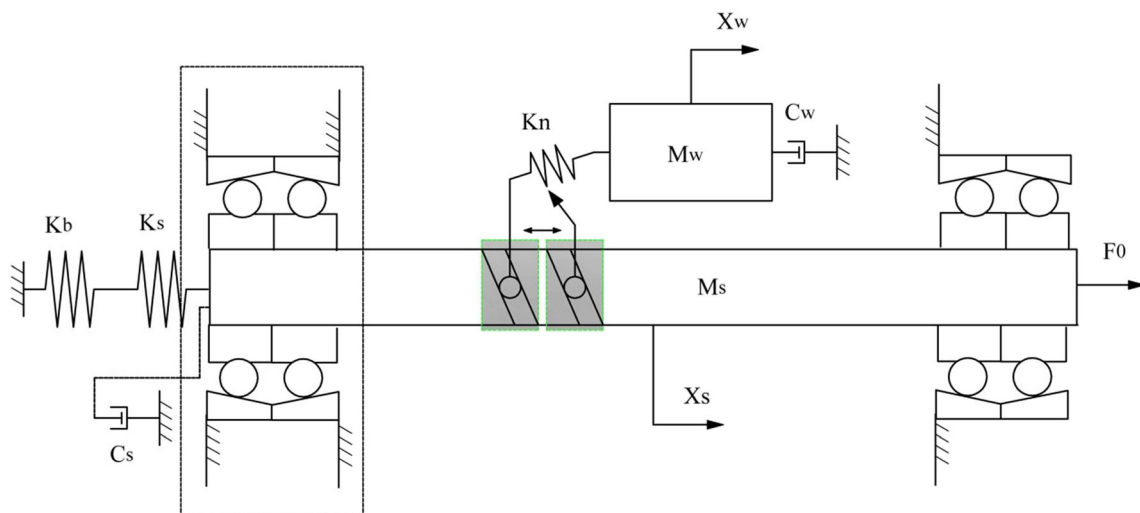


Fig. 3 Modeling of the ball screw system with a lumped parameter system

The following iterative form of solving Eq. 5 is rewritten as

$$\begin{aligned} & \frac{1}{s^2} T_{j+1}^{k+1} - \left(\frac{2}{s^2} + \frac{\rho c}{k} \frac{1}{\tau} \right) T_j^{k+1} + \frac{1}{s^2} T_{j-1}^{k+1} \\ & = -\frac{\rho c}{k} \frac{1}{\tau} T_j^k + \frac{Ph}{kA_c} T_j^k - \frac{Ph}{kA_c} T_{air} \end{aligned} \tag{20}$$

The forced convective coefficient h is rewritten as [40]

$$h = 0.133 \left(\frac{\pi n}{60v} \right)^{\frac{2}{3}} d_s^{\frac{1}{3}} P_r^{\frac{1}{3}} \tag{21}$$

Determining thermal elongation of the screw shaft During the feed working, the axial thermal elongation of a screw shaft is always produced, for the temperature of the screw caused by frictional heat increases.

Hence, based on the result of real-time modeling of the temperature arising of the screw shaft, the expression of thermal elongation of the screw shaft can be obtained as:

$$\Delta L = \alpha_s \int_0^L \Delta T(x, t) dx \tag{22}$$

where $\Delta T(x, t)$ denotes the temperature rise of the screw shaft, and α_s denotes the thermal expansion coefficient.

The axial deformation caused by the friction heat mainly affects the preloads and of the stiffness of the systems.

Calculating the rest tensile preload Because of the thermal elongation of the screw shaft, the rest tensile preload is described as,

$$F_{ap} = F_0 - \Delta F_0 \tag{23}$$

Table 1 Parameters of the feed drive system

Parameters	Given value
Working table mass M_w	450 kg
Ball screw mass, M_s	5 kg
Lead of screw P	10 mm
Nut length	80 mm
Nut type	Single nut
Bearing type	Contact ball bearing
Lubrication	Grease
Thermal conductivity k	43.3W/m °C
Material density of the ball screw ρ	7800kg/m ³
Coefficient of linear thermal expansion α	1.2 × 10 ⁻⁵ /°C
Damping coefficient of the guide way C_w	10 Ns/m
Damping coefficient of the supporting bearing C_s	10 Ns/m
Diameter of the ball screw shaft d_r	0.032 m
Displacement of the working table x_w	um
Axial displacement of the ball screw x_s	um

Determining the axial stiffness of the circle bar Considering that the tensile preload variation influences the screw stiffness, the axial stiffness of the circle bar is defined as

$$k_s = \frac{PS_s E}{(P - F_{ap})x} \tag{24}$$

where P is the external axial load.

2.1.3 Stiffness of the supporting system

The stiffness of the screw supporting system consists of the stiffness of support bearing and the axial stiffness of the screw shaft, which are connected in series. Hence, the stiffness of the supporting system is written as

$$k_e = \frac{k_s k_b}{k_s + k_b} \tag{25}$$

2.2 Screw-nut stiffness model

The axial contact stiffness between the ball screw shaft and the nut is given by [41]

$$k_n = 0.8 \left(\frac{F_{n0}}{\varepsilon C_a} \right)^{1/3} K \tag{26}$$

2.3 Ball screw system governing equation

In order to investigate the dynamic characteristics of the ball screw system varying with the different increment of temperature, the entire system is modeled, as shown in Fig. 3. The system is composed of the screw shaft, working table, and supporting bearings.

To consider the effects of the different increment of temperature, the supporting system stiffness and the screw-nut stiffness are treated as variables.

The matrix[M] is written as

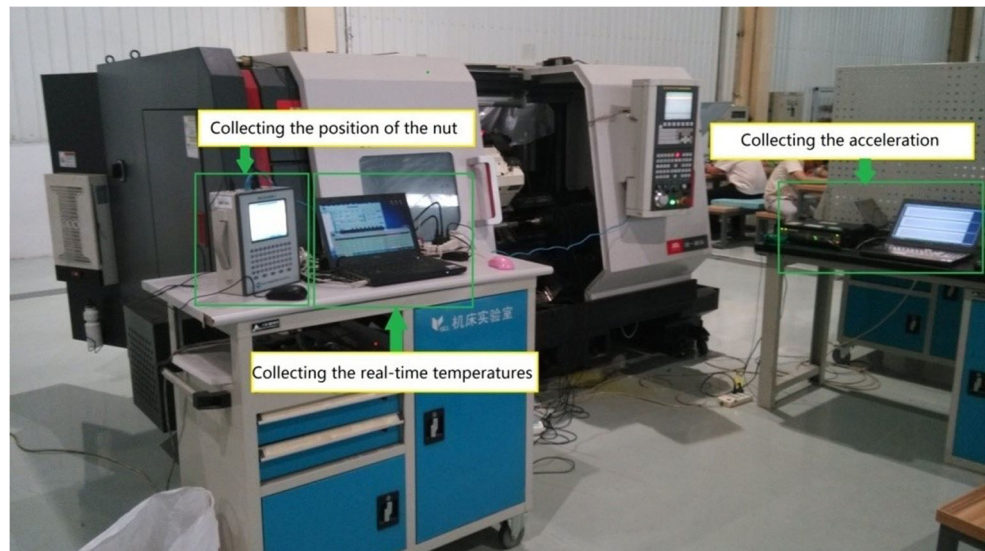
$$[M] = \begin{bmatrix} M_w & 0 \\ 0 & M_s \end{bmatrix} \tag{27}$$

The matrix[C] is written as

$$[C] = \begin{bmatrix} C_w & 0 \\ 0 & C_s \end{bmatrix} \tag{28}$$

The matrix[K] is written as

Fig. 4 Experimental setup



$$[K] = \begin{bmatrix} k_n & -k_n \\ -k_n & k_n + k_e \end{bmatrix} \tag{29}$$

The vector X is written as

$$X = \begin{bmatrix} x_w \\ x_s \end{bmatrix} \tag{30}$$

The vector F is written as

$$F = \begin{bmatrix} 0 \\ 0 \end{bmatrix} \tag{31}$$

The matrix [M], [C], and [K] are the system mass, the system damping, and the system stiffness matrix, respectively. [F] is the excitation force vector, and [X] is the displacement vector.

Combining Eqs. 27–31, the system governing equation can be presented as the matrix form

$$[M]\{\ddot{X}\} + [C]\{\dot{X}\} + [K]\{X\} = \{F(t)\} \tag{32}$$

2.4 Solving dynamic model

This model belongs to a SDOF system. The parameters of the feed drive system were listed in Table 1. Through taking the Laplace transform of all the equations and summarizing the results in matrix form, the dynamic characteristics were obtained.

2.4.1 Axial natural frequency of the working table

The axial natural frequency of the working table is obtained as

$$\omega_w = \frac{1}{2M_1M_2} \left\{ \sqrt{2} \left[M_1M_2 (k_eM_1 + k_nM_1 + k_nM_2 + \sqrt{k_e^2M_1^2 + 2k_ek_nM_1^2 - 2k_ek_nM_1M_2 + k_n^2M_1^2 + 2k_n^2M_1M_2 + k_n^2M_2^2}) \right]^{1/2} \right\} \tag{33}$$

2.4.2 Axial natural frequency of the screw

The axial natural frequency of the screw is obtained as

$$\omega_s = \frac{1}{2M_1M_2} \left\{ \sqrt{2} \left[M_1M_2 (k_eM_1 + k_nM_1 + k_nM_2 - \sqrt{k_e^2M_1^2 + 2k_ek_nM_1^2 - 2k_ek_nM_1M_2 + k_n^2M_1^2 + 2k_n^2M_1M_2 + k_n^2M_2^2}) \right]^{1/2} \right\} \tag{34}$$

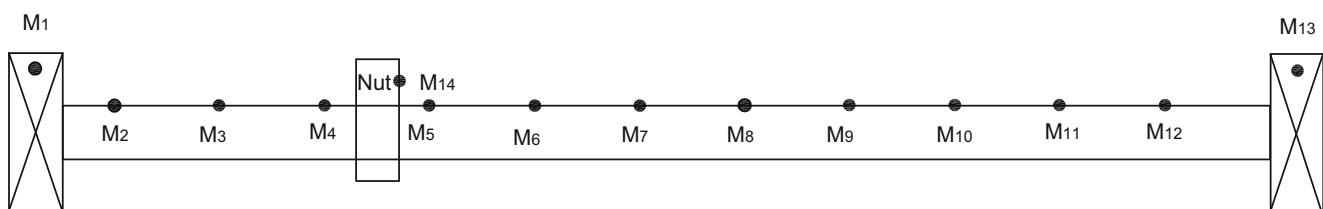


Fig. 5 Measuring location arrangement

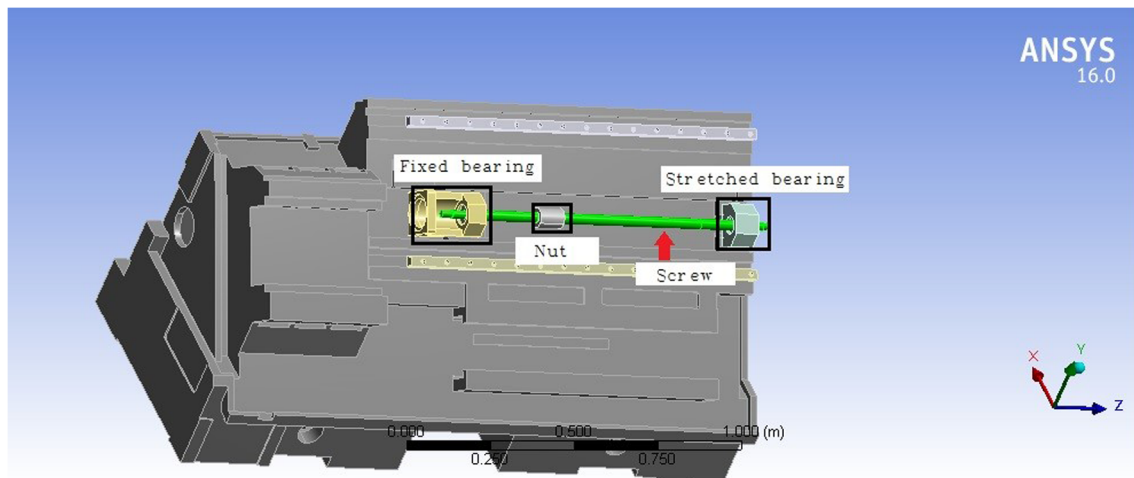


Fig. 6 Thermal dynamic identification model of the ball screw feed drive system

3 Experimental verification and dynamics simulation for ball screw feed drives

3.1 Experimental verification

3.1.1 Experimental setup

In order to investigate the thermal characteristics of the ball screw feed drive system, experiments were performed on CNC machine tools; the z-axis feed system was tested under different feed rates. Figure 4 shows the experimental setup of testing the screw system.

The experimental setup of the lathe consists of an infrared thermal imaging instrument, a temperature collecting instrument with four thermocouples, a computer with the Visual C++ FOCAS application, a computer with LAMS software, and a CNC lathe.

3.1.2 Sensor locations

In order to investigate the temperature characteristics of the system, experiments were carried out using the measuring location arrangement shown in Fig. 5. The 14 testing points of temperature were shown in Fig. 5. The 1st, 13th, and 14th testing points were respectively located on the surfaces of bearing seat 1, the surfaces of bearing seat 2, and the flank surface of the nut, and the three points were measured by three thermocouples, respectively. The testing points (2–12) of temperature on the screw shaft (shown in Fig. 5) is evenly taken every 42 mm from the reference origin point of the machine tool up to 420 mm. The ball screw system is warmed up by the repeated movement of the nut along the screw shaft, between points 2 and 12. To measure the measuring point temperature in the stroke of the ball screw shaft, an infrared thermal imaging instrument was selected.

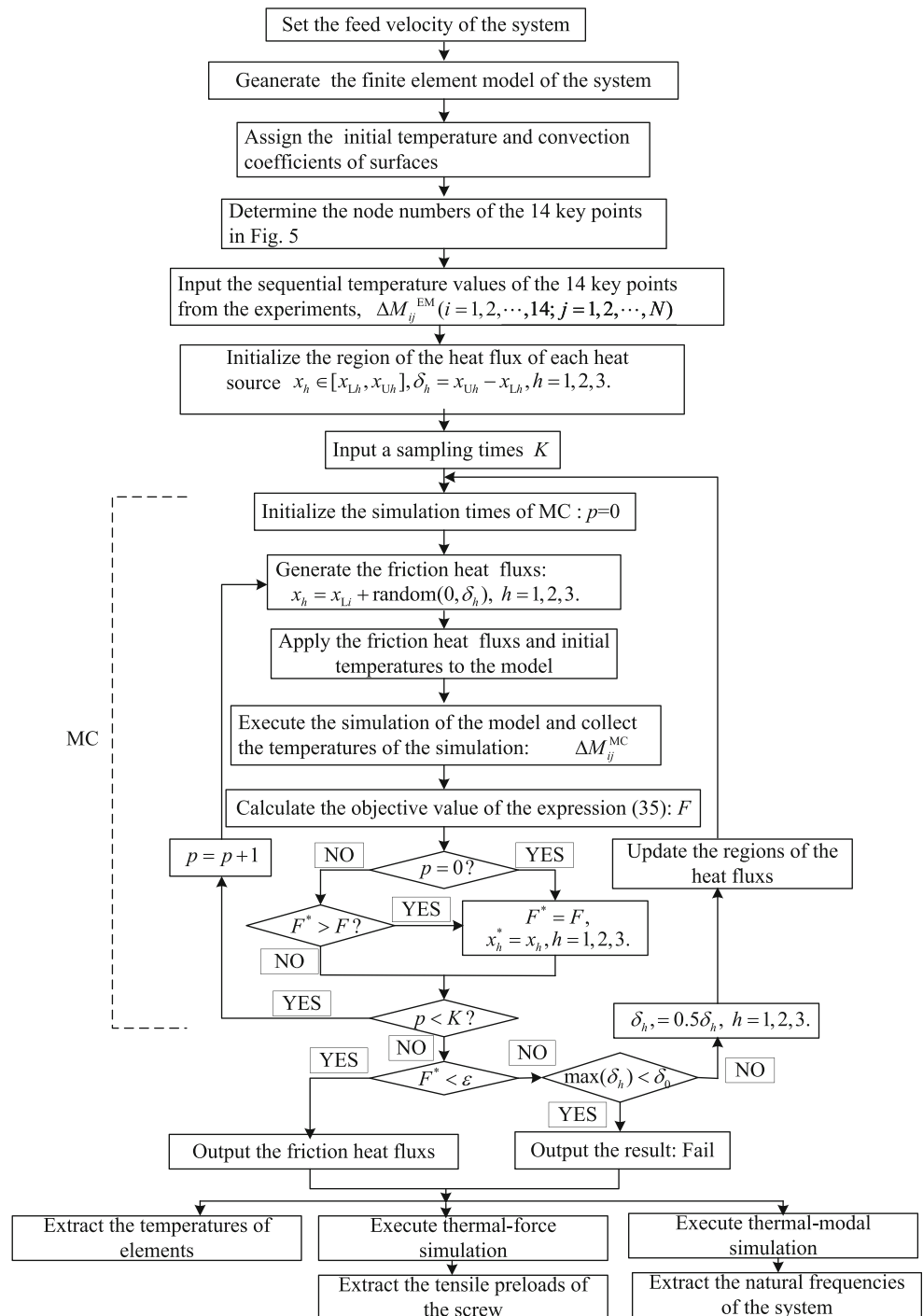
3.1.3 Testing procedure

The z-axis feed drive of a lathe was tested using no load. First, the CNC lathe was initially begun, and the initial characteristics were collected. After this, by moving the worktable repeatedly in its stroke range, the ball screw feed system of the CNC lathe was heated. Meanwhile, the temperature of the bearings, and moving-nut was collected using the thermocouples at an interval of 0.048 s. Temperature of the screw shaft was taken using a thermal imaging instrument at an interval of 10 min. After the lathe was warmed up for 10, 20, 30, 40, and 50 min, the natural frequencies of the carriage were measured using LAMS. To obtain the position of the moving-nut, an application program based on the FOCAS was used to collect the real-time position of the carriage in sampling intervals of 0.048 s.

3.2 Inverse identification method of the heat excitation

In order to study the thermal dynamic performance deeply, this paper proposed an inverse identification method of the heat excitation, as shown in Fig. 6. To obtain the heat flow rates of the fixed bearing 1, the stretched bearing 2, and the moving-nut, the Monte Carlo method is used. Once the MC process is completed, the FEM process is preformed to obtain the temperature field of the ball system. In order to capture the three heat flow rates, experiments were performed to obtain the temperature rise of 14 designated points, which are denoted by M1, M2, ..., M14 in Fig. 5. The method to obtain the heat flow rates of three heat sources is that the temperature rises of the FEM calculation agrees with the data measured by experiments. The calculating process can search the heat flow rates, through minimizing the following expression:

Fig. 7 Flow diagram of the thermal dynamic identification model of the ball screw feed drive system



$$F(x_1, x_2, x_3) = \sum_i \sum_j \left(\Delta M_{ij}^{EM} - \Delta M_{ij}^{MC} \right)^2 \tag{35}$$

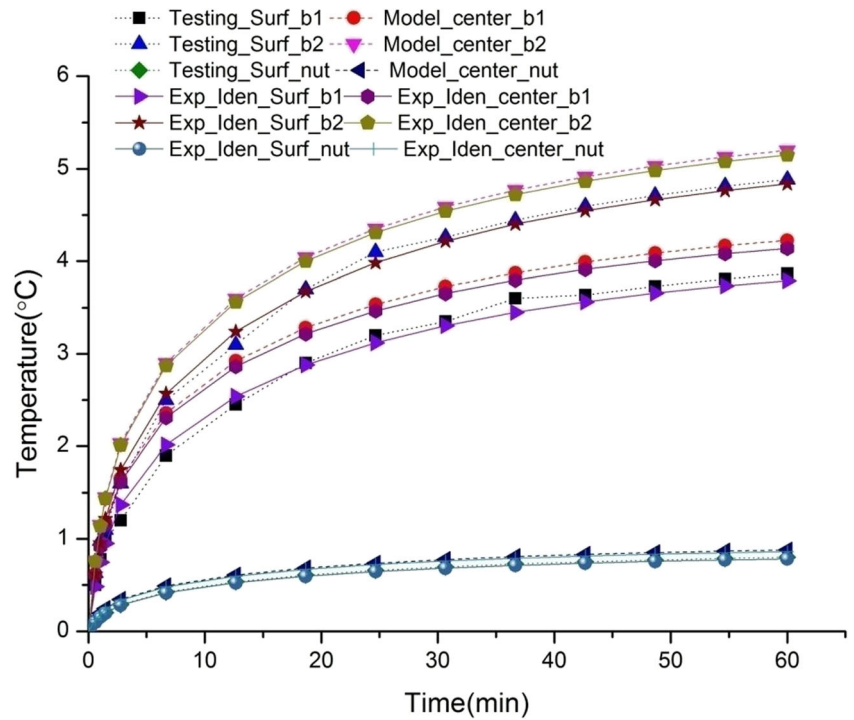
where ΔM_{ij}^{EM} denotes the measured temperature for given point i at the j th sampling time step of t_j , $i = 1, 2, \dots, 14$, and $j = 1, 2, \dots, N$, ΔM_{ij}^{MC} denotes the simulated temperature for given point i at the j th sampling time step of t_j , $i = 1, 2, \dots, 14$,

and $j = 1, 2, \dots, N$. Figure 7 shows the flow diagram of the thermal dynamic identification model of the ball screw feed drive system.

The thermal dynamic identification process of the ball screw feed drive system is as follows:

1. Generating the thermal dynamic finite element model of the system according to the geometric dimension of the ball screw feed drive system.

Fig. 8 Comparison of key point temperatures of the thermal dynamic model, experiments, and inverse identification by experiments of the ball screw feed drive system



2. Inputting the initial temperature, convention coefficient, and the thermal flux regions of the fixed bearing, stretched bearing, and nut $x_h \in [x_{Lh}, x_{Uh}]$, $\delta_h = x_{Uh} - x_{Lh}$, $h = 1, 2, 3$.
3. Using the Monte Carlo method, the friction heat fluxes $x_h = x_{Lh} + \text{random}(0, \delta_h)$, $h = 1, 2, 3$, are generated.
4. Executing the simulation of the model and collect the 14 key temperatures of the simulation.
5. Calculating the objective value of the expression (35): F and search the minimum objective value of the expression (35): F^*
6. If F^* is less than the setting small value \mathcal{E} , the friction heat fluxes are obtained. If F^* is bigger than the setting small value \mathcal{E} , the regions of the friction heat fluxes are updated, and repeated the MC process until F^* is less than the setting small value \mathcal{E} .
7. Extracting the temperatures of elements.
8. Executing thermal-force simulation and extract the tensile preloads of the screw.
9. Executing thermal-modal simulation and extract the natural frequencies of the system.

Fig. 9 Comparison of tensile preloads of the dynamic model and inverse identification

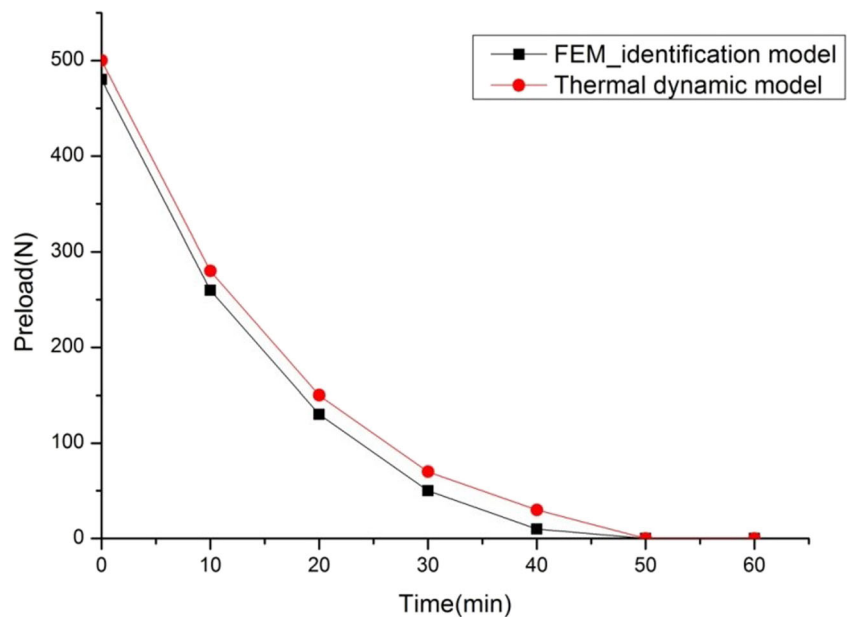
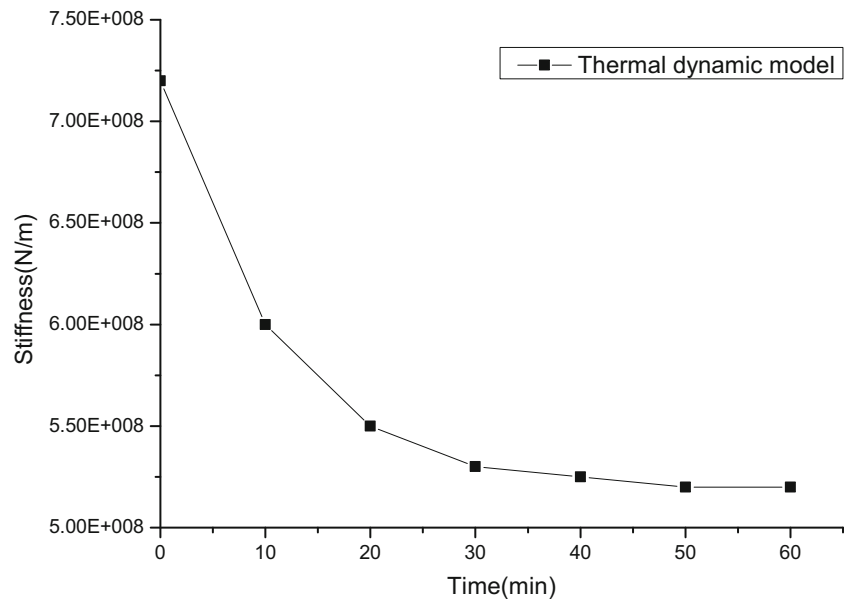


Fig. 10 Axial supporting stiffness of the screw system sharply decreases at the position of 336 mm (obtained by the thermal dynamic model)



4 Results and discuss

In order to verify the thermal model, the tests of machine tools were conducted at Z axis positions, under the different increment of temperature of the screw using the feed rate 5 m/min.

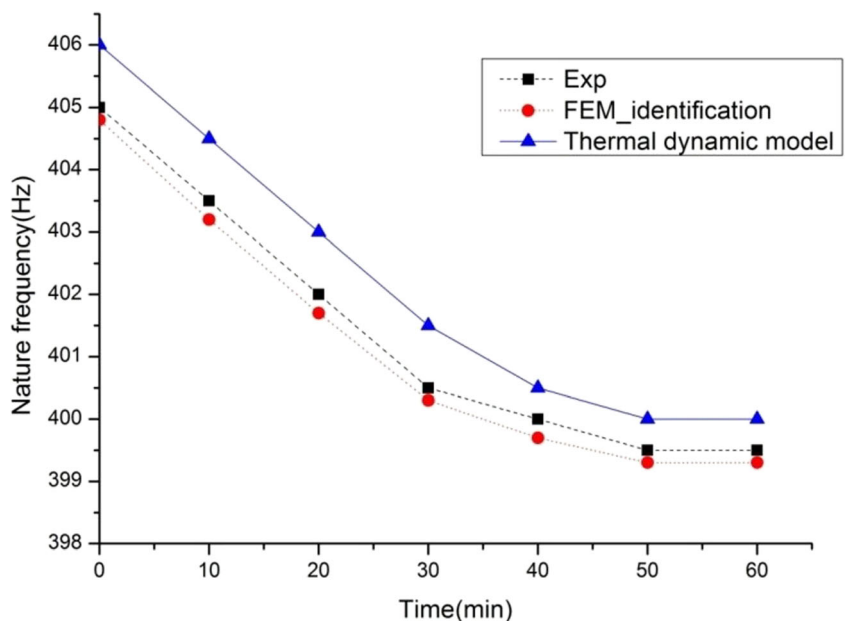
4.1 Temperature distribution of the screw system

In order to investigate the thermal dynamic performance of ball screws, the temperature distribution of the screw system is necessary.

The comparison of key point temperatures of the thermal dynamic model, experiments, and inverse identification by experiments of the ball screw feed drive system was shown in Fig. 8.

The point line denotes the measured temperature of testing points of the bearings and nut, the solid line denotes temperature from the inverse identification of the testing points and the centers of the bearings and nut, and the dash line denotes the temperature obtained by the thermal dynamic model of the centers of the bearings and nut. The results shows that the temperature rise of the inverse identification by experiments agrees with the data of the experiments, and the temperature

Fig. 11 Comparison of the natural frequencies of working table for the dynamic model, inverse identification, and experiments at the position of 336 mm



rise of the thermal dynamic model agrees with the data of the inverse identification by experiments under the feed rate 5 m/min. The effectiveness of the proposed thermal dynamic model was proved through the above results.

4.2 Preload variation of the screw due to temperature increase

The thermally induced axial deformation of the screw certainly affects the preload, which changes the dynamic performance of the ball screw system.

Figure 9 shows that comparison of tensile preloads of the dynamic model and inverse identification method. From the results, it is can be seen that the tensile preload of system sharply decreases with the increase of temperature. The calculated results of the model could match quite well with the inverse identification results. During ball screw systems working, due to the increase of temperature, the thermal deformation increases, which causes the decrease of the tensile preload of the screw shaft.

4.3 Variation of the stiffness and natural frequency due to temperature increase

The thermally induced axial deformation of the screw certainly affects the supporting system stiffness and the natural frequency, which changes the dynamic performance of the ball screw system.

According to the dynamic model, the axial supporting stiffness of the working table at Z axis position of 336 mm is obtained under the feed rate 5 m/min. Figure 10 shows that the axial supporting stiffness of the working table nonlinearly decreases with the increase of temperature. This is because the decrease of the tensile preload of the screw shaft causes the system axial stiffness nonlinearly changes.

Using the above solutions Eqs. 33 and 34 of the dynamic model, the dynamic characteristics varying with the temperature of the screw system was exposed. And the natural frequencies of the working table at Z axis position of 336 mm was measured under the feed rate 5 m/min.

Figure 11 shows the comparison of natural frequencies of the dynamic model, inverse identification, and experiments. From the results, it can be seen that the natural frequency of system slowly decreases. The calculated results of the model could match quite well with the actual measured results and inverse identification.

This is because in the working stage, the tensile preload of system sharply decreases, the axial stiffness of system sharply decreases, and the natural frequency of system slowly decreases.

The experimental results and analytical solution results showed the effective of the proposed dynamic model. The proposed dynamic model has been validated in the testing machine tool.

5 Conclusions

Based on the analysis of the preloads and stiffness of the feed drive system varying with temperature rise, a new lumped, thermally induced dynamic model has been successfully presented for studying the dynamic performance due to the temperature variation of the ball screw feed drive system.

1. A new analytical model of the real-time temperature field of a hollow cylinder with the varied heat flow was proposed, based on the heat theory. By using the thermocouples to read the surface temperatures of heat sources, this model can be used to obtain the real-time temperature field of the bearings and moving-nut.
2. A new finite difference heat transfer model with real-time moving heat sources was proposed. By using the FOCAS function to read the real-time position of moving heat sources, this model can be used to obtain the temperature distribution of the screw. Based on this model, the real-time thermally induced preloads and stiffness models of the ball screw system were obtained. Furthermore, an analytical real-time thermally induced dynamic model of the ball screw system has been successfully presented, and the analytical solutions of this model were obtained.
3. An inverse identification method of the heat excitation was proposed. Using this method and experiments, the relationships between the preload, axial stiffness, and natural frequency and the temperature variation of the ball screw system were investigated. The extension preload and the axial stiffness markedly decrease with the increase of temperature. However, the natural frequency slowly decreases with the increase of temperature. The results proved that the effectiveness of the presented thermal dynamic models. These models provided the theoretical and practical foundation of the real-time monitoring and controlling of dynamic characteristics of preloaded ball screw systems. These methods focus on real-time thermal dynamic characteristics of preloaded ball screw systems, which can be used for other machines by suitable modification.

Funding information This work was supported by the National Natural Science Foundation of China under Grants 51775085 and U1708254.

References

1. Verl A, Frey S (2010) Correlation between feed velocity and preloading in ball screw drives. *CIRP Ann Manuf Technol* 59(1): 429–432
2. Oyanguren A, Larrañaga J, Ulacia I (2018) Thermo-mechanical modeling of ball screw preload force variation in different working conditions. *Int J Adv Manuf Technol* 97(1-4):723–739

3. Mohring HC, Bertram O (2012) Integrated autonomous monitoring of ball screw drives. *CIRP Ann Manuf Technol* 61:355–358
4. Altintas Y, Verl A, Brecher C, Uriarte L, Pritschow G (2011) Machine tool feed drives. *CIRP Ann* 61(2):779–796
5. Cheng CC, Shiu JS (2001) Transient vibration analysis of a high-speed feed drive system. *J Sound Vib* 239(3):489–504
6. Chen JS, Huang YK, Cheng CC (2004) Mechanical model and contouring analysis of high-speed ball-screw drive systems with compliance effect. *Int J Adv Manuf Technol* 24:241–250
7. Hsieh MF, Yao WS, Chiang CR (2007) Modeling and synchronous control of a single-axis stage driven by dual mechanically-coupled parallel ball screws. *Int J Adv Manuf Technol* 34(9-10):933–943
8. Erkorkmaz K, Altintas Y (2001) High speed CNC system design. Part II: modeling and identification of feed drives. *Int J Mach Tools Manuf* 41:1487–1509
9. Jerzy Z (2012) Vibration of the ball screw drive. *Eng Fail Anal* 24:1–8
10. Li B, Luo B, Mao XY, Cai H, Peng FY, Liu HQ (2013) A new approach to identifying the dynamic behavior of CNC machine tools with respect to different worktable feed speeds. *Int J Mach Tools Manuf* 72:73–84
11. Feng GH, Pan YL (2012) Investigation of ball screw preload variation based on dynamic modeling of a preload adjustable feed-drive system and spectrum analysis of ball-nuts sensed vibration signals. *Int J Mach Tools Manuf* 52:85–96
12. Zhou CG, Feng HT, Chen ZT, Ou Y (2016) Correlation between preload and no-load drag torque of ball screws. *Int J Mach Tools Manuf* 102:35–40
13. Frey S, Dadalau A, Verl A (2012) Expedient modeling of ball screw feed drives. *Prod Eng Res Devel* 6:205–211
14. Frey S, Walther M, Verl A (2010) Periodic variation of preloading in ball screws. *Prod Eng Res Dev* 4(2–3):261–267
15. Vicente DA, Hecker RL, Villegas FJ, Flores GM (2012) Modeling and vibration mode analysis of a ball screw drive. *Int J Adv Manuf Technol* 58:257–265
16. Wei CC, Lai RS (2011) Kinematical analyses and transmission efficiency of a preloaded ball screw operating at high rotational speeds. *Mech Mach Theory* 46:880–898
17. Varanasi KK, Nayfeh S (2004) The dynamics of lead-screw drives: low-order modeling and experiments. *J Dyn Syst Meas Control (ASME)* 126:388–396
18. Kamalzadeh A, Erkorkmaz K (2007) Compensation of axial vibrations in ball screw drives. *Ann CIRP* 56(1):373–378
19. Xia JY, Wu B, Hu YM, Shi TL (2010) Experimental research on factors influencing thermal dynamics characteristics of feed system. *Precis Eng* 34:357–368
20. Xia JY, Hu YM, Wu B, Shi TL (2009) Research on thermal dynamics characteristics and modeling approach of ball screw. *Int J Adv Manuf Technol* 43(5-6):421–430
21. Bryan J (1990) International status of thermal error research. *CRIP Ann-Manuf Technol* 39(2):645–656
22. Yun WS, Kim SK, Cho DW (1999) Thermal error analysis for a CNC lathe feed drive system. *Int J Mach Tools Manuf* 39:1087–1101
23. Ramesh R, Mannan MA, Po AN (2003) Thermal error measurement and modeling in machine tools. Part I Influence of varying operation condition, *Int J Mach Tools Manuf* 43:391–404
24. Xu ZZ, Liu XJ (2011) Thermal error forecast and performance evaluation for an air-cooling ball screw system. *Int J Mach Tools Manuf* 51:605–611
25. Min X, Jiang S (2010) A thermal model of a ball screw feed drive system for a machine tool. *Proceedings of the Institution of Mechanical Engineers Part C Journal of Mechanical Engineering Science* 225:186–192
26. Li ZH, Fan KG (2014) Time-varying positioning error modeling and compensation for ball screw systems based on simulation and experimental analysis. *Int J Adv Manuf Technol* 73(5-8):773–782
27. Liang RJ, Ye WH, Haiyan H, Yang QF (2012) The thermal error optimization models for CNC machine tools. *Int J Adv Manuf Technol* 63(9-12):1167–1176
28. Xu ZZ, Liu XJ (2014) Study on thermal behavior analysis of nut/shaft air cooling ball screw for high-precision feed drive. *Int J Precis Eng Manuf* 15:123–128
29. Zhang Y, Yang JG, Jiang H (2012) Machine tool thermal error modeling and prediction by grey Neural network. *Int J Adv Manuf Technol* 59(9-12):1065–1072
30. Wu CW, Tang CH, Chang CF, Shiao YS (2012) Thermal error compensation method for machine center. *Int J Adv Manuf Technol* 59:681–689
31. Han J, Wang LP, Wang HT (2012) A new thermal error modeling method for NC machine tools. *Int J Adv Manuf Technol* 62:205–212
32. Vyroubal J (2012) Compensation of machine tool thermal deformation in spindle axis direction based on decomposition method. *Precis Eng* 36(1):121–127
33. Zhang T, Ye WH, Shan YC (2016) Application of sliced inverse regression with fuzzy clustering for thermal error modeling of CNC machine tool. *Int J Adv Manuf Technol* 85:2761–2771
34. Liu K, Li TJ, Sun MJ, Wu YL, Zhu TJ (2018) Physically based modeling method for comprehensive thermally induced errors of CNC machining centers. *Int J Adv Manuf Technol* 94(1-4):463–474
35. Liu K, Li T, Li TJ, Liu Y, Wang YQ, Jia ZJ (2018) Thermal behaviour analysis of horizontal CNC lathe spindle and compensation for radial thermal drift error. *Int J Adv Manuf Technol* 95(1-4):1293–1301
36. Oyanguren A, Zahn P, Alberdi AH, Larrañaga J, Lechler A, Ulacia I (2016) Preload variation due to temperature increase in double nut ball screws. *Prod Eng Res Devel* 10:529–537
37. Horejs O (2007). Thermo-mechanical model of ball screw with non-steady heat sources. *International Conference on Thermal Issues in Emerging Technologies: Theory & Application* IEEE133-137
38. Navarro y de Sosa I, Bucht A, Junker T, Pagel K, Drossel WG (2014) Novel compensation of axial thermal expansion in ballscrew drives. *Prod Eng Res Dev* 8(3):397–406
39. Yang SM, Tao WQ (2006) Heat transfer. Beijing. Higher education press 52-53[in Chinese]
40. Li TJ, Zhao CY, Zhang YM (2018) Adaptive real-time model on thermal error of ball screw feed drive systems of CNC machine tools. *Int J Adv Manuf Technol* 94(9-12):3853–3861
41. Hiwin Technologies Company (2000) Hiwin ball screw technical information. Hiwin Company, Taiwan

Publisher's note Springer Nature remains neutral with regard to jurisdictional claims in published maps and institutional affiliations.